

Experimental realization of a ballistic spin interferometer based on the Rashba effect using a nanolithographically defined square loop array

Takaaki Koga^{1,2,3,*}, Yoshiaki Sekine², and Junsaku Nitta^{2,3†}

¹*PRESTO, Japan Science and Technology Agency,*

4-1-8, Honchou, Kawaguchi, Saitama, 332-0012, Japan

²*NTT Basic Research Laboratories, NTT Corporation,*

3-1, Morinosato-Wakamiya, Atsugi, Kanagawa, 243-0198, Japan

³*CREST, Japan Science and Technology Agency,*

4-1-8, Honchou, Kawaguchi, Saitama, 332-0012, Japan

The gate-controlled electron spin interference was observed in nanolithographically defined square loop (SL) arrays fabricated using $\text{In}_{0.52}\text{Al}_{0.48}\text{As}/\text{In}_{0.53}\text{Ga}_{0.47}\text{As}/\text{In}_{0.52}\text{Al}_{0.48}\text{As}$ quantum wells. In this experiment, we demonstrate electron spin precession in quasi-one-dimensional channels that is caused by the Rashba effect. It turned out that the spin precession angle θ was gate-controllable by more than 0.75π for a sample with $L = 1.5\mu\text{m}$, where L is the side length of the SL. Large controllability of θ by the applied gate voltage as such is a necessary requirement for the realization of the spin FET device proposed by Datta and Das [Datta *et. al.*, Appl. Phys. Lett. **56**, 665 (1990)] as well as for the manipulation of spin qubits using the Rashba effect.

PACS numbers: 71.70.Ej, 73.20.Fz, 73.23.Ad, 73.63.Hs

Exploitation of spin degree of freedom for the conduction carriers provides a key strategy for finding new functional devices in semiconductor spintronics [1, 2, 3, 4, 5, 6]. A promising approach for manipulating spins in semiconductor nanostructures is the utilization of spin-orbit (SO) interactions. In this regard, lifting of the spin degeneracy in the conduction (or valence) band due to the structural inversion asymmetry is especially called the ‘‘Rashba effect’’ [7, 8], the magnitude of which can be controlled by the applied gate voltages and/or specific design of the sample heterostructures [9, 10].

Recently, we proposed a ballistic spin interferometer (SI) using a square loop (SL) geometry, where an electron spin rotates by an angle θ due to the Rashba effect as it travels along a side of the SL ballistically [11]. In a simple SI model, an incident electron wave to the SI (see Fig. 1 in Ref. 11) is split by a ‘‘hypothetical’’ beam splitter into two partial waves, where each of these partial waves follows the SL path in the clockwise (CW) and counter-clockwise (CCW) directions, respectively. Then, they interfere with each other when they come back to the incident point (at the beam splitter). As a consequence, the incident electron would either scatter back on the incident path (called ‘‘path1’’) or emerge on the other path (called ‘‘path2’’). The backscattering probability to path1 (P_{back}) for the case that the incident elec-

tron is spin unpolarized is given by [11],

$$\begin{aligned} P_{\text{back}} &= \frac{1}{2} + \frac{1}{4} (\cos^4\theta + 4\cos\theta\sin^2\theta + \cos 2\theta) \cos\phi \\ &\equiv \frac{1}{2} + A(\theta)\cos\phi, \end{aligned} \quad (1)$$

where ϕ is the quantum mechanical phase due to the vector potential responsible for the magnetic field \mathbf{B} piercing the SL ($\phi = 2eBL^2/\hbar$, L being the side length of the SL) and θ is the spin precession angle when the electron propagates through each side of the SL due to the Rashba effect ($\theta = 2\alpha m^*L/\hbar^2$, α and m^* being the Rashba SO coupling constant and the electron effective mass, respectively). A plot of $A(\theta)$ as a function of θ is found in Ref. 11. We note that $A(\theta)$ corresponds to the amplitude of the Al’tshuler-Aronov-Spivak(AAS)-type oscillation of electric conductance experimentally [12]. Equation (1) predicts that the amplitude of the AAS oscillation should be modulated as a function of θ , which, in turn, can be controlled by the applied gate voltage V_g through the variation of the α values.

In this Letter, we present the first experimental demonstration of the SI using nanolithographically defined SL arrays in epitaxially grown (001) $\text{In}_{0.52}\text{Al}_{0.48}\text{As}/\text{In}_{0.53}\text{Ga}_{0.47}\text{As}/\text{In}_{0.52}\text{Al}_{0.48}\text{As}$ quantum wells (QW). Details of the sample preparation are following: we use the same MOCVD-grown epi-wafers of $\text{In}_{0.52}\text{Al}_{0.48}\text{As}/\text{In}_{0.53}\text{Ga}_{0.47}\text{As}/\text{In}_{0.52}\text{Al}_{0.48}\text{As}$ QWs as those we used for the weak antilocalization (WAL) study previously (samples1-4 in Ref. 10). We first exploit the electron beam lithography (EBL) and electron cyclotron resonance (ECR) plasma etching techniques to define an array of SLs in the area of $150 \times 200 \mu\text{m}^2$. We then use the photolithography and wet etching techniques to form a Hall bar mesa of the size of $125 \times 250 \mu\text{m}^2$ over the SL array regions. In this way, the area of the final SL array region in the Hall bar mesa

*Electronic address: koga@ist.hokudai.ac.jp; Present address: Graduate School of Information Science and Technology, Hokkaido University, Sapporo, 060-0814, Japan

†Present address: Graduate School of Engineering, Tohoku University, Sendai, 980-8579, Japan

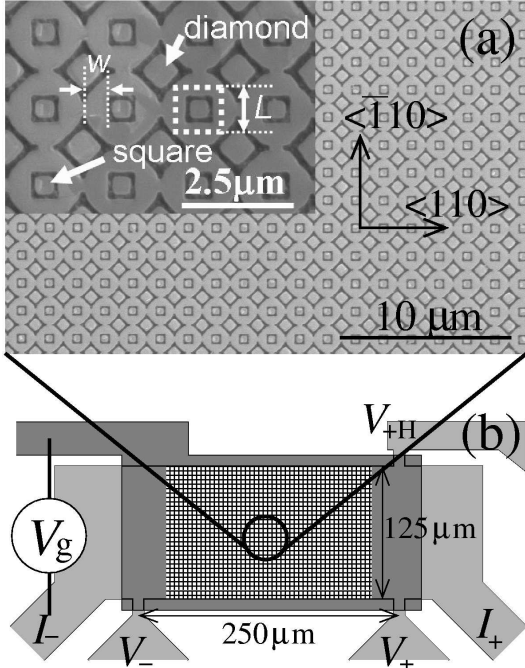


FIG. 1: (a) SEM micrographs of the nanolithographically defined square loop array ($L = 1.2\mu\text{m}$). A two-dimensional electron gas exists in the relatively light regions. (b) Schematic diagram for the Hall bar sample used in the present experiment.

is $125 \times 200 \mu\text{m}^2$ [see Fig. 1(b)]. These samples have a gate electrode (Au) covering the entire Hall bar, using a 100 nm thick SiO_2 layer as a gate insulator, which makes it possible to control the sheet carrier density N_S and the Rashba spin-orbit parameter α by the applied gate voltage V_g . We note that all the measurements were carried out at $T = 0.3$ K using a ^3He cryostat, exploiting the conventional ac lock-in technique. When the electric sheet conductivities σ_{2D} of these samples were measured [using the electrodes labeled by I_+ , I_- , V_+ and V_- in Fig. 1(b)] as a function of B ($\mathbf{B} \perp$ to the sample surface) for a given V_g [denoted as $\sigma_{2D}(B)$], the Hall voltages were also measured using the electrodes labeled by V_+ and V_{+H} . In this way, we were able to monitor $\sigma_{2D}(B)$ and N_S at the same time for each given V_g . We then investigate the amplitude of the AAS oscillations at $B = 0$ [denoted as $\Delta\sigma_{2D}(B = 0)$], as a function of V_g (equivalently N_S), to test the prediction of the SI [11].

Examples of the scanning electron micrographs (SEM) of the SL pattern used in the present experiment are shown in Fig. 1(a). We note that electrons exist in the relatively lighter regions of the picture. The relatively darker lines and curves that define the “diamond” (\diamond) and “square” (\square) shapes in Fig. 1(a), are the dry-etched regions by the ECR plasma etching. We note that electrons exist in these diamond- and square-shaped islands. However, these islands do not contribute to the

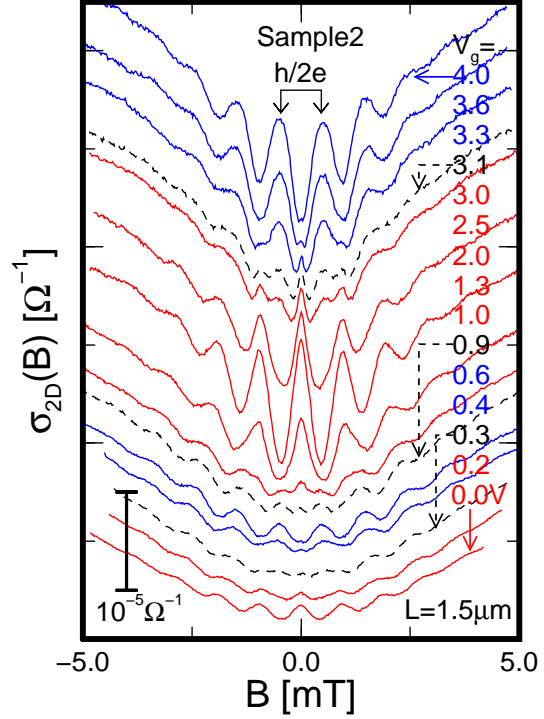


FIG. 2: Gate voltage dependence of the electric sheet conductivities σ_{2D} as a function of the magnetic field B for a square loop (SL) array sample ($L = 1.5\mu\text{m}$) fabricated using the sample2 epi-wafer in Ref. 10. The plotted curves are shifted along y axis for the ease of comparison. The magnitudes of σ_{2D} at $B = 0$ range from $3.7 \times 10^{-4} \Omega^{-1}$ (for $V_g = 0.0$ V) to $10.3 \times 10^{-4} \Omega^{-1}$ (for $V_g = 4.0$ V). The range of B (ΔB) that corresponds to the magnetic flux half quanta piercing the SL ($\Delta B \times L^2 = h/2e$) is indicated by “ $h/2e$ ” in the figure.

electric conductivity, since they are not electrically connected one another. We sketch a SL path for the spin interference by the dotted white square in the inset of Fig. 1(a), where electrons would be localized if the type of the spin interference is constructive. The width W of the SL path is also defined in Fig. 1(a). We used $W = 0.5\mu\text{m}$ throughout the present experiment. We can see that these SLs are electrically connected with the neighboring SLs. As a result, they contribute to the electric conductivity of the whole Hall bar.

Shown in Fig. 2 is the gate voltage (V_g) dependence of $\sigma_{2D}(B)$ for a SL array sample ($L = 1.5\mu\text{m}$) that is fabricated using the sample2 epi-wafer in Ref. 10. Here, we clearly see the AAS oscillations, whose period (ΔB) is given by $h/2eL^2$. We also note that as the value of V_g is increased from 0.0 V, the peak feature in $\sigma_{2D}(B)$ at $B = 0$ become dip across $V_g = 0.3$ V [a dashed $\sigma_{2D}(B)$ curve]. Then, the dip feature becomes peak for $V_g > 0.9$ V [also indicated by another dashed $\sigma_{2D}(B)$ curve]. Finally the peak feature again becomes dip for $V_g > 3.1$ V. Thus the amplitudes of the AAS oscillations at $B = 0$ oscillate as a function of V_g as predicted in Eq. (1).

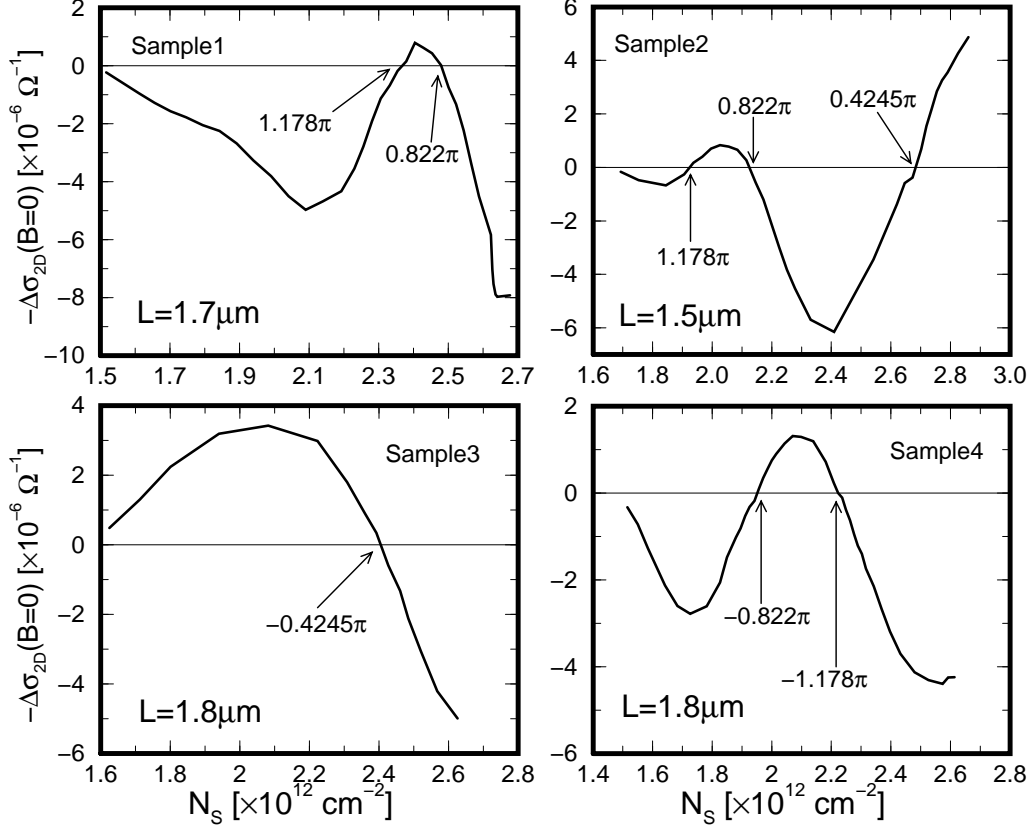


FIG. 3: Amplitudes of the experimental AAS oscillations at $B = 0$ measured for various SL array samples ($L = 1.5 - 1.8 \mu\text{m}$ using the sample 1–4 epi-wafers introduced in Ref. 10) plotted as a function of the sheet carrier density N_S . θ values at the node positions (denoted as θ^* in the text) are also given. We plot $-\Delta\sigma(B = 0)$ instead of $\Delta\sigma(B = 0)$ to match the signs of the values with those for $A(\theta)$ given in Eq. (1).

Plotted in Fig. 3 are the amplitudes of the experimental AAS oscillation at $B = 0$ [denoted as $\Delta\sigma_{2D}(B = 0)$] as a function of N_S for the SI devices fabricated using the sample 1–4 epi-wafers ($L = 1.7$ and $1.5 \mu\text{m}$ for samples 1 and 2, respectively, and $L = 1.8 \mu\text{m}$ for samples 3 and 4), where we employed the Fast Fourier Transform (FFT) and inverse FFT techniques to extract only the oscillatory part of σ whose period corresponds to the magnetic flux half quanta $h/2e$. We indeed see that $-\Delta\sigma(B = 0)$ oscillates with N_S , where we observe several nodes. Using the α vs. N_S relations that are obtained from the WAL analysis of an unpatterned QW sample and the $\mathbf{k} \cdot \mathbf{p}$ model calculation using appropriate boundary conditions [10], θ values for sample 2 at these node positions [denoted as θ^* below], for example, are identified as (from left to right) 1.178π , 0.822π and 0.4245π (see Fig. 2 in Ref. 11). We thus demonstrated that the spin precession angle θ is gate-controllable by more than 0.75π for a length of $1.5 \mu\text{m}$. The θ^* values for the other SI devices using the other epi-wafers are also identified in Fig. 3. We can, then, calculate the α values at these node positions using the relation $\alpha = \theta^* \hbar^2 / 2m^* L$.

In Fig. 4, we plot the α values obtained in this way (denoted as α_{SI}) for various SL array samples made of the sample1-4 epi-wafers as a func-

tion of N_S . Also plotted in Fig. 4 are (1) the α values obtained from the WAL analysis of the unpatterned (bare) Hall bars (denoted as α_{WAL}) and (2) those obtained from the $\mathbf{k} \cdot \mathbf{p}$ model calculations (denoted as $\alpha_{\mathbf{k} \cdot \mathbf{p}}$) using the appropriate boundary conditions and assuming the presence of the background impurities [10]. We note that the unpatterned Hall bars for α_{WAL} are prepared on the same wafer pieces as those used for the SL array samples. We also note that in Ref. 10 we obtained $\alpha_{\mathbf{k} \cdot \mathbf{p}}$ values without assuming the background impurities and found quantitatively good agreement with α_{WAL} values. In the present work, we included the effect of the background impurities (mostly they are present in the $\text{In}_{0.52}\text{Al}_{0.48}\text{As}$ buffer layer) in the model calculation of $\alpha_{\mathbf{k} \cdot \mathbf{p}}$ to better fit the experimental α_{WAL} and α_{SI} values. It turned out that the values of the background impurity densities obtained from these fittings are reasonably small (typically $1 \times 10^{16} \text{ cm}^{-3}$). The details of this analysis are discussed elsewhere [13].

In summary, we have demonstrated experimentally the electron spin interference phenomena based on the Rashba effect, which are predicted previously [11]. For this demonstration, we prepared nanolithographically defined square loop array structures in $\text{In}_{0.52}\text{Al}_{0.48}\text{As}/\text{In}_{0.53}\text{Ga}_{0.47}\text{As}/\text{In}_{0.52}\text{Al}_{0.48}\text{As}$

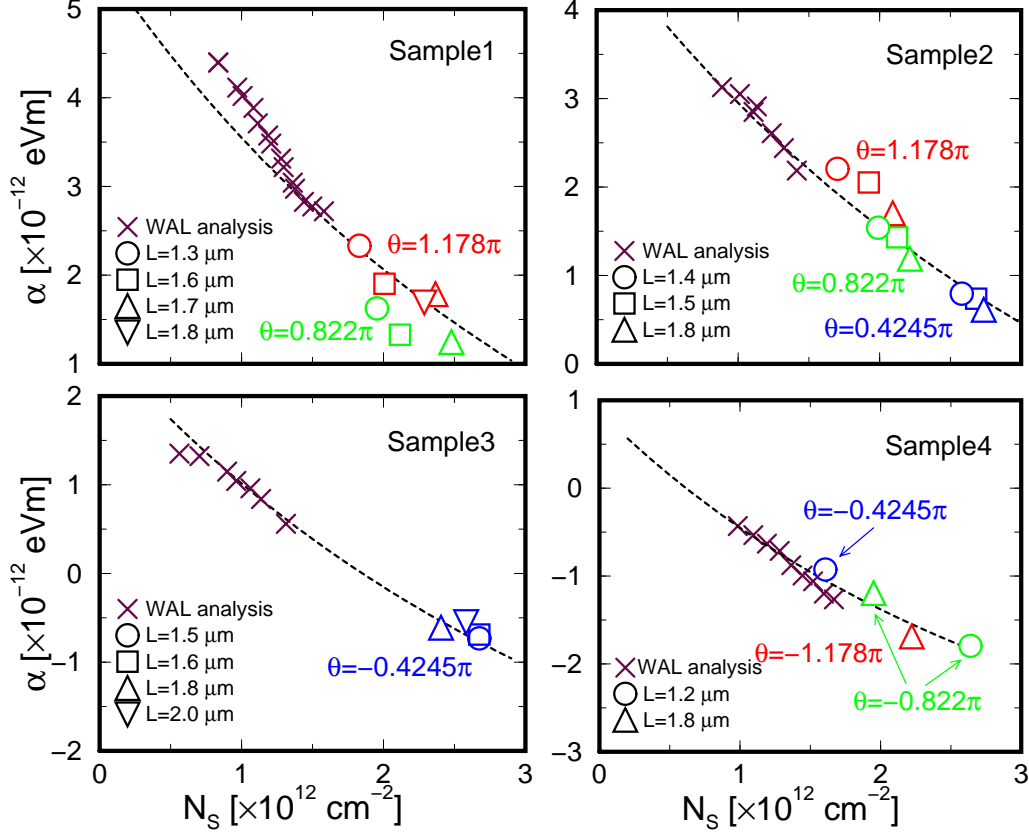


FIG. 4: The values of the Rashba spin-orbit parameter α , for four different epi-wafers denoted as samples1-4 in Ref. 10, deduced from the three independent analyses: (1) the weak antilocalization analysis (crosses), (2) the analysis of the node positions in the $-\Delta\sigma_{2D}(B=0)$ vs. N_S relations for the square loop arrays using the relation $\alpha = \theta\hbar^2/2m^*L$ (various symbols) and (3) the $\mathbf{k} \cdot \mathbf{p}$ model calculations using appropriate boundary conditions (dashed curves). The background impurity densities (N_i) assumed for the $\mathbf{k} \cdot \mathbf{p}$ calculations are $N_i = 1 \times 10^{16}$, 4×10^{16} , 1.4×10^{16} and 1×10^{16} cm $^{-3}$ for samples 1–4, respectively.

quantum wells using the electron beam lithography and ECR dry etching techniques and measured the low-field magnetoresistances of these samples ($\mathbf{B} \perp$ sample surface) at low temperatures (0.3 K). We observed the Al'tshuler-Aronov-Spivak (AAS) oscillations, whose magnitudes at $B = 0$ oscillated as a function of the gate voltage as the result of the spin interference. We also deduced the α values

(Rashba spin-orbit coupling constant) from the analysis of the spin interferometry experiments. We obtained quantitative agreements among (1) the α values obtained from the spin interferometry experiments, (2) those obtained from the weak antilocalization analysis, and (3) those obtained from the $\mathbf{k} \cdot \mathbf{p}$ model calculations.

-
- [1] D. Awschalom, N. Samarth, and D. Loss, *Semiconductor Spintronics and Quantum Computation* (Springer Verlag, 2002).
- [2] S. Datta and B. Das, *Appl. Phys. Lett.* **56**, 665 (1990).
- [3] T. Koga, J. Nitta, H. Takayanagi, and S. Datta, *Phys. Rev. Lett.* **88**, 126601 (2002).
- [4] J. Nitta, F. E. Meijer, and H. Takayanagi, *Appl. Phys. Lett.* **75**, 695 (1999).
- [5] D. Bercioux, M. Governale, V. Cataudella, and V. M. Ramaglia, *Phys. Rev. Lett.* **93**, 056802 (2004).
- [6] Y. K. Kato, R. C. Myers, A. C. Gossard, and D. D. Awschalom, *Appl. Phys. Lett.* **86**, 162107 (2005).
- [7] E. I. Rashba, *Sov. Phys. Solid State* **2**, 1109 (1960), [*Fiz. Tverd. Tela (Leningrad)* **2**, 1224 (1960)].
- [8] Y. A. Bychkov and E. I. Rashba, *J. Phys. C* **17**, 6039 (1984).
- [9] J. Nitta, T. Akazaki, H. Takayanagi, and T. Enoki, *Phys. Rev. Lett.* **78**, 1335 (1997).
- [10] T. Koga, J. Nitta, T. Akazaki, and H. Takayanagi, *Phys. Rev. Lett.* **89**, 046801 (2002).
- [11] T. Koga, J. Nitta, and M. van Veenhuizen, *Phys. Rev. B* **70**, 161302(R) (2004).
- [12] B. L. Al'tshuler, A. G. Aronov, and B. Z. Spivak, *JETP Lett.* **33**, 94 (1981).
- [13] Y. Sekine, T. Koga, and J. Nitta, (2005), unpublished.